AIP Journal of Applied Physics

# Poling effect and piezoelectric response in high-strain ferroelectric 0.70 Pb ( Mg 1 / 3 Nb 2 / 3 ) O 3 – 0.30 PbTiO 3 crystal

H.-Y. Chen, C.-S. Tu, C.-M. Hung, R. R. Chien, V. H. Schmidt, C.-S. Ku, and H.-Y. Lee

Citation: Journal of Applied Physics **108**, 044101 (2010); doi: 10.1063/1.3475150
View online: http://dx.doi.org/10.1063/1.3475150
View Table of Contents: http://scitation.aip.org/content/aip/journal/jap/108/4?ver=pdfcov
Published by the AIP Publishing

# Poling effect and piezoelectric response in high-strain ferroelectric $0.70Pb(Mg_{1/3}Nb_{2/3})O_3-0.30PbTiO_3$ crystal

H.-Y. Chen,[1] C.-S. Tu,[1,2,a)] C.-M. Hung,[2] R. R. Chien,[3] V. H. Schmidt,[3] C.-S. Ku,[4] and H.-Y. Lee[4]
[1]*Department of Physics, Fu Jen Catholic University, Taipei 242, Taiwan*
[2]*Graduate Institute of Applied Science and Engineering, Fu Jen Catholic University, Taipei 242, Taiwan*
[3]*Department of Physics, Montana State University, Bozeman, Montana 59717, USA*
[4]*National Synchrotron Radiation Research Center, Hsinchu Science Park, Hsinchu 30076, Taiwan*

(Received 7 March 2010; accepted 3 July 2010; published online 18 August 2010)

*In situ* high-resolution synchrotron x-ray diffraction, dielectric permittivity, hysteresis loop, and polarization current, were used to investigate phase transitions of (211)-cut $0.70Pb(Mg_{1/3}Nb_{2/3})O_3-0.30PbTiO_3$ single crystal before and after an electric ($E$) field poling. A rhombohedral (R)–tetragonal (T)–cubic transition sequence was observed upon zero-field heating in both unpoled and poled samples. Before the R–T transition takes place, an extra dielectric and polarization current anomalies near 365 K were observed in the poled sample due to a transition of polarization ordering. The direct piezoelectric coefficient $d_{33}$ exhibits a rapid increase for poling at $E=1.0-1.3$ kV/cm, followed by an overpoling behavior. The increment of polarization ordering plays an important role while the high piezoelectric response builds up. © *2010 American Institute of Physics*. [doi:10.1063/1.3475150]

## I. INTRODUCTION

Nanostructures or polar nanoregions have been considered as the most important feature in relaxor ferroelectrics because they play an important role in ferroelectric (FE) properties. Nuclear-magnetic-resonance study of the prototype relaxor $Pb(Mg_{1/3}Nb_{2/3})O_3$ (PMN) showed two components in the crystal matrix, i.e., isotropic spherical glass matrix and anisotropic FE nanoclusters.[1] The FE polar nanostructures which can respond to an external $E$ field, embed in the single-dipole-glass matrix which does not respond appreciably to an $E$ field.[1] Neutron and x-ray results revealed that the bulk unit cell of PMN remains cubic (C) for poling field $E<8.0$ kV/cm.[2] A long-range polar order was suggested in PMN from the reduction in diffuse scattering intensity below $T_C$ under an $E$ field.[2] Different structures between the outer layer (10–50 $\mu$m) and the interior have been observed in $(1-x)Pb(Zn_{1/3}Nb_{2/3})O_3-xPbTiO_3$ (PZN–PT) and PMN–PT crystals.[3–8] A skin effect of 10–50 $\mu$m thickness was revealed in PZN–PT crystals for $0\leq x\leq 8.0$, in which the near-surface region and interior bulk exhibit different structures.[4] PMN–10%PT and PMN–20%PT transform to a X phase instead of rhombohedral (R) phase below $T_C$.[6] R phase was observed in the outer layer and interior in PMN–27%PT, suggesting that the ground state of PMN–PT crystal interior prefers the X phase for small Ti content, and becomes R phase as Ti increases.

Based on the high-resolution x-ray diffraction (XRD), phase diagrams of (001) and (110) PMN–PT crystals for $0.15\leq x\leq 0.38$ have been proposed upon field-cooling (FC).[9] The C–$M_A$, C–(tetragonal) T–$M_A$, C–T–$M_C$, and C–T FC phase transitions under $E=0.25-0.5$ kV/cm were observed from the (001) PMN–PT crystals, respectively, for $x<0.25$, $0.25\leq x\leq 0.30$, $0.30\leq x\leq 0.35$, and $x>0.35$.[9] Here, $M_A$, $M_B$, $M_C$, and O are various monoclinic phases and orthorhombic phase, respectively. However, (110) PMN–PT crystals exhibit the C–$M_B$, C–O–$M_B$, C–T–O–$M_B$, C–T–O, and C–T FC phase transitions under $E=0.25-2$ kV/cm, respectively, for $x<0.20$, $0.22\leq x\leq 0.30$, $x\cong 0.3$, $0.31\leq x\leq 0.36$, and $x>0.35$.[9] Neutron and XRD results revealed that PMN–32%PT behaves a similar temperature-dependent soft mode as in PMN, suggesting that soft-mode dynamics in PMN–PT are independent of Ti content on the Ti-poor side.[10]

For piezoelectric performance, an $E$ field poling is usually employed before application. How a prior $E$ field poling affects phase thermal stability and piezoelectric response is still an important subject in the high-strain relaxor FE crystals. An additional phase was often induced after an $E$ field poling, which depends on orientation and poling strength.[11–13] From the dielectric result of the (110) PMN–33%PT crystal, a R–O–T–C phase transition was proposed upon heating after poling at $E<4$ kV/cm along [110].[12] An $E$-induced R–O transition was suggested for $E>5$ kV/cm.[12] An $E$-induced (111) R–(110) O transition through $M_B$-type distortion was proposed for a (110) PMN–30%PT crystal.[13]

In high-strain relaxor FE crystals,[14,15] piezoelectric coefficients often show a rapid rise with poling field $E_p$ in the range of 1–3 kV/cm, perhaps followed by a reduction at larger $E_p$ due to the overpoling effect. Understanding the origin of this rapid increase in piezoresponse with $E_p$ is essential for piezoelectric applications. In this report, we point out that piezoelectric coefficient can be nonzero only if the average spontaneous polarization is nonzero, and that this is main reason for the rapid rise of $d_{33}$ from zero as $E_p$ is increased.

a)Electronic mail: 039611@mail.fju.edu.tw.

 

## II. EXPERIMENTAL PROCEDURE

The PMN–30%PT crystal was grown using a modified Bridgman method. A Wayne-Kerr Analyzer PMA3260A was used to obtain the real part $\varepsilon'$ of dielectric permittivity. The sample was cut perpendicular to a ⟨211⟩ direction and its basal surfaces were sputtered with gold electrodes. Three processes were used in dielectric measurements. The first two are called "zero-field-heated" (ZFH) and "zero-field-cooled" (ZFC), in which the data were taken upon heating and cooling without an $E$ field. In "prior-poled before ZFH" (PP-ZFH), the sample was poled at room temperature with a dc $E=5$ kV/cm along [211], then ZFH was performed. ZFH and PP-ZFH processes were also used in the polarization current measurements as denoted by $J_{ZFH}$ and $J_{PP\text{-}ZFH}$ by using a Keithley 6517A electrometer. Hysteresis loops were taken by using a Sawyer–Tower circuit at $f=46$ Hz.

*In situ* high-resolution (211) synchrotron XRD was performed at the National Synchrotron Radiation Research Center (in Taiwan) with photon energy of 8.0 keV ($\lambda=1.550$ Å). To avoid surface stress caused by polishing, thin gold films were deposited and were kept on the sample after poling. The XRD spectra were fitted by using the sum of Gaussian and Lorentzian terms. The XRD $2\theta$-reflection and $d$ spacing obey the Bragg law, $2d_{hkl}\sin\theta_{hkl}=n\lambda$. The $d$ values for the six T domain types can be calculated from the equation, $1/d^2=(h^2+k^2)/a_T^2+(l^2/c_T^2)$, where $(h,k,l)$ and $(a_T,c_T)$ are crystallographic orientation and lattice parameters. The six T domain types have two different $d$ spacings from the (211) reflections, i.e., $d_{(211)}=(5/a_T^2+1/c_T^2)^{-1/2}$ and $d_{(112)}=(2/a_T^2+4/c_T^2)^{-1/2}$. For the eight R domain types, three $d$ spacings are expected from the (211) reflections, i.e., $d_{(211)}=\beta/[6\sin^2\alpha+10(\cos^2\alpha-\cos\alpha)]^{1/2}$, $d_{(21\bar{1})}=\beta/[6\sin^2\alpha-2(\cos^2\alpha-\cos\alpha)]^{1/2}$, and $d_{(2\bar{1}\bar{1})}=\beta/[6\sin^2\alpha-6(\cos^2\alpha-\cos\alpha)]^{1/2}$.[16] Here $\beta$ is $a_R(1-3\cos^2\alpha+2\cos^3\alpha)^{1/2}$.

The direct (or normal) piezoelectric coefficient $d_{33}$ was measured by using a Model ZJ-6B Quasi-Static Piezo Meter. Before each $d_{33}$ measurement, the sample was poled with a dc $E$ field along [211] at room temperature. $d_{33}$ was obtained by measuring the surface charge density under a sine-wave stress along [211].

## III. RESULTS AND DISCUSSION

Figure 1 shows (a) ZFH dielectric permittivity $\varepsilon'_{ZFH}$ and ZFH polarization current density $J_{ZFH}$, (b) PP-ZFH dielectric permittivity $\varepsilon'_{PP\text{-}ZFH}$, and (c) PP-ZFH polarization current density $J_{PP\text{-}ZFH}$. The dielectric maxima and corresponding temperatures are nearly the same ($T_m\cong415$ K) in both ZFH and PP-ZFH. The $\varepsilon'_{ZFH}$ exhibits a gradual steplike anomaly near 385 K followed by a steep-rise shoulder near 405 K. These anomalies correlate with a narrow thermal hysteresis over the wide range of 280–400 K as shown in the inset of Fig. 1(a). The ZFC permittivity is slightly higher than the ZFH permittivity. This implies that as the crystal cools, some of the disordered relaxor material gradually transforms to macrodomains which are electrically stiffer and upon subsequent heating the macrodomains do not transform back reversibly to relaxor material. A small dip followed by a strong

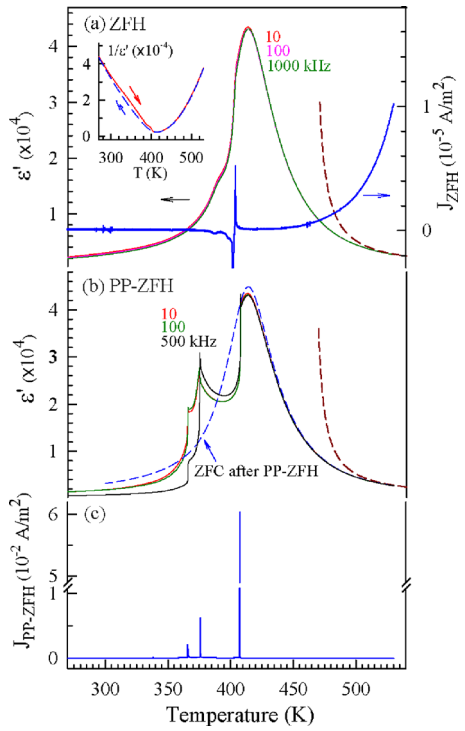


FIG. 1. (Color online) (a) ZFH dielectric permittivity $\varepsilon'_{ZFH}$ and ZFH polarization current density $J_{ZFH}$ (with the scale at right vertical axis), (b) PP-ZFH dielectric permittivity $\varepsilon'_{PP\text{-}ZFH}$ and $\varepsilon'_{ZFC}$ ($f=10$ kHz) after the PP-ZFH, and (c) PP-ZFH polarization current density $J_{PP\text{-}ZFH}$. The inset in (a) is $1/\varepsilon'$ from ZFH and ZFC processes.

down-and-up spike in $J_{ZFH}$ reveals pronounced changes in polarization ordering near 385 and 405 K. The weak $J_{ZFH}$ current density comes from the difference in positively and negatively randomly oriented domains or spontaneous polarization $P_S$, i.e., $J_{ZFH}=-\partial P_S/\partial t$.

$\varepsilon'_{PP\text{-}ZFH}$ and $J_{PP\text{-}ZFH}$ exhibit three corresponding discontinuous anomalies near 365, 375, and 408 K below $T_m\cong415$ K, indicating a sequence of polarization transitions. The $J_{PP\text{-}ZFH}$ mainly associates with thermal decay of the $E$-induced polarization $P_{ind}$, i.e., $J_{PP\text{-}ZFH}=-\partial P_{ind}/\partial t$. Note that $\varepsilon'_{PP\text{-}ZFH}\cong1800$ is lower than $\varepsilon'_{ZFH}\cong2600$ at room temperature for $f=10$ kHz. This difference implies that the prior poling along [211] induces a polarized state which already has a large polarization component along [211] and thus reduces dielectric response under the weak [211] measuring field.

How can these PP-ZFH dielectric and polarization current results be explained? First, note that the *in situ* synchrotron XRD result (which will be discussed later) reveals an enhancement of R phase ordering along (211) after poling at $E=5.0$ kV/cm. As temperature is raised to 365 K, there is a transition of polarization ordering from one R state to another due to a change in $d$ spacing or ion displacement. The transition at 375 K is presumed to be a first-order R–T transition as evidenced in the synchrotron XRD, which exhibits a change in $d$ spacing at 375 K. The first-order nature is consistent with the discontinuities in $\varepsilon'_{PP\text{-}ZFH}$ and $J_{PP\text{-}ZFH}$ at this transition, and with the eighth-order Landau expansion result.[17]

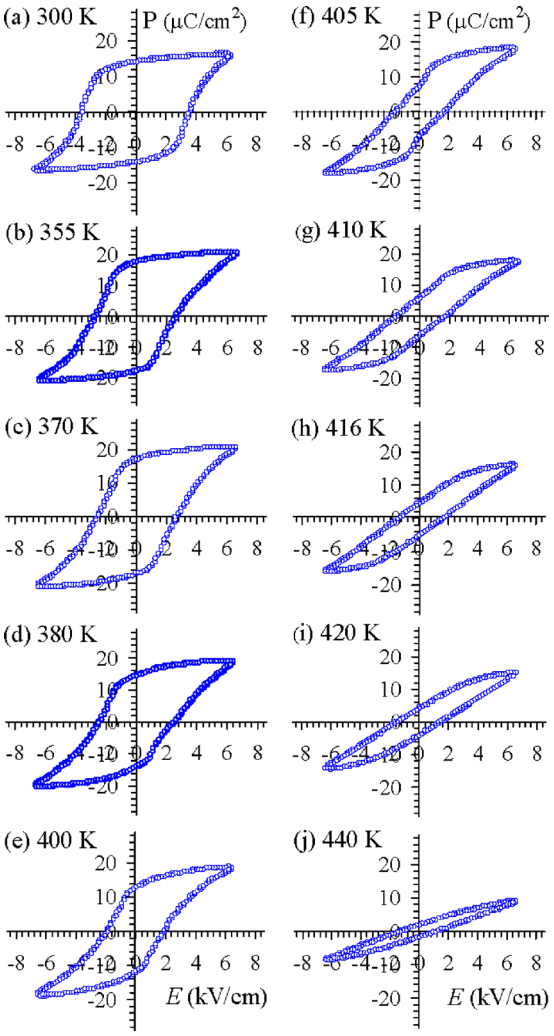


FIG. 2. (Color online) Hysteresis loops upon heating.

Both $\varepsilon'_{ZFH}$ and $\varepsilon'_{PP\text{-}ZFH}$ were found to follow the Curie–Weiss equation, $\varepsilon' = C/(T - T_o)$, above 510 K, below which there is noticeable deviation from the Curie–Weiss law. The dashed lines in Figs. 1(a) and 1(b) are fittings with the same Curie–Weiss constants $C = 1.8 \times 10^5$ K and $T_o = 465$ K. We consider 510 K to be the Burns temperature ($T_B$), below which dipole glass attenuates dielectric response and polar nanoclusters begin to develop.[18] The weaker dielectric response of dipole glass causes deviation from the Curie–Weiss law and the polar nanoclusters are responsible for the weak frequency dispersion.[19] The ZFC dielectric permittivity measured after the PP-ZFH [Fig. 1(b)] shows the same behavior as seen in $\varepsilon'_{ZFC}$ [Fig. 1(a)], indicating that the *E*-induced polarized state can be thermally erased.

Figure 2 shows hysteresis loops upon heating. The remanent polarization ($P_r$) and coercive field ($E_C$) are, respectively, about 14 $\mu C/cm^2$ and 3.5 kV/cm at room temperature. In Fig. 3, $P_r$ exhibits a local maximum plateau at 350–365 K, indicating that the crystal reaches a maximum polarization before a rapid decline. With anomalies in $\varepsilon'_{PP\text{-}ZFH}$ and $J_{PP\text{-}ZFH}$ near 365 K, these results suggest that the *E*-induced [211] R domain underwent a transition of polarization ordering near 365 K. The obvious change in slope of $E_C$ and the steep decline of $P_r$ near 375 K is consistent with

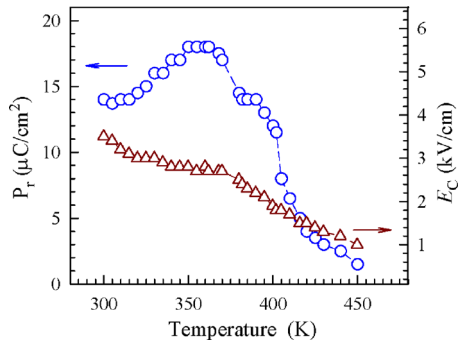


FIG. 3. (Color online) Remanent polarization ($P_r$) and coercive field ($E_C$) upon heating.

anomalies observed in $\varepsilon'_{PP\text{-}ZFH}$ and $J_{PP\text{-}ZFH}$ that we interpreted as a first-order R–T phase transition. The fractional drop of polarization near 375 K is consistent with the fraction $\sqrt{2/3} = 0.8165$ expected for the component of [100] T polarization along [211]. Upon further heating, $P_r$ exhibits another steep decline in the region of 405–415 K. The polarization appears to retain some finite magnitude above $T_m \cong 415$ K as seen commonly in disordered FE materials but this could result from a field-induced transition under an ac *E* field application. In addition, three upward responses in $J_{PP\text{-}ZFH}$ near 365, 375, and 408 K can be explained by the negative slopes of polarization (Fig. 3) in the corresponding temperature regions, i.e., $J_{PP\text{-}ZFH} = -(\partial P_{ind}/\partial T)(\partial T/\partial t)$. Here, *T* and *t* are temperature and time. Note that $\partial T/\partial t$ is positive upon heating.

The ZFH (211) synchrotron XRD are given in Fig. 4, in which two peaks are observed at 298 K. Three possible *d* spacings are expected from the (211) reflections for the eight R domain types, i.e., $d_{(211)}$, $d_{(21\bar{1})}$, and $d_{(2\bar{1}\bar{1})}$. The lattice parameters of $a_R = 4.0253$ Å and $\alpha = 89.904°$ of the R phase calculated from $d_{(211)}$ and $d_{(2\bar{1}\bar{1})}$ are consistent with $a = 4.0275$ Å and $\alpha = 89.906°$ obtained previously from the (111) PMN–30%PT crystal.[20] Fig. 5 shows the temperature-dependent *d* spacing and lattice parameters upon heating. As temperature increases, the two *d* spacings of R phase gradually approach each other and then exhibit a discontinuous change in slope near 380 K, which corresponds to anomalies in $\varepsilon'_{ZFH}$ and $J_{ZFH}$. The angle $\alpha$ of R phase shifts toward 90° near 380 K, confirming an R–T transition.

The lattice parameter $c_T$ of T phase exhibits a change in slope near 400 K, indicating a transition of polarization ordering. This can explain the rapid rise and spike near 405 K in $\varepsilon'_{ZFH}$ and $J_{ZFH}$. The two *d* spacings of T phase join together near $T_m = 415$ K, indicating that the crystal enters into the C phase. The gradual increase of *d* spacing in the C phase is due to thermal expansion. In brief, the (211) unpoled PMN–30%PT crystal undergoes a R–T–C transition sequence at 380 and 415 K upon zero-field heating.

PP-ZFH (211) XRD spectra are given in Fig. 6 and show a single peak at 298 K, which corresponds to the (211) reflection of R phase. This indicates that the (211) peak was enhanced significantly after poling along [211]. This (211) R peak exhibits an upward shift in *d* spacing as temperature approaches 365 K (Fig. 7), implying a transition of polariza-

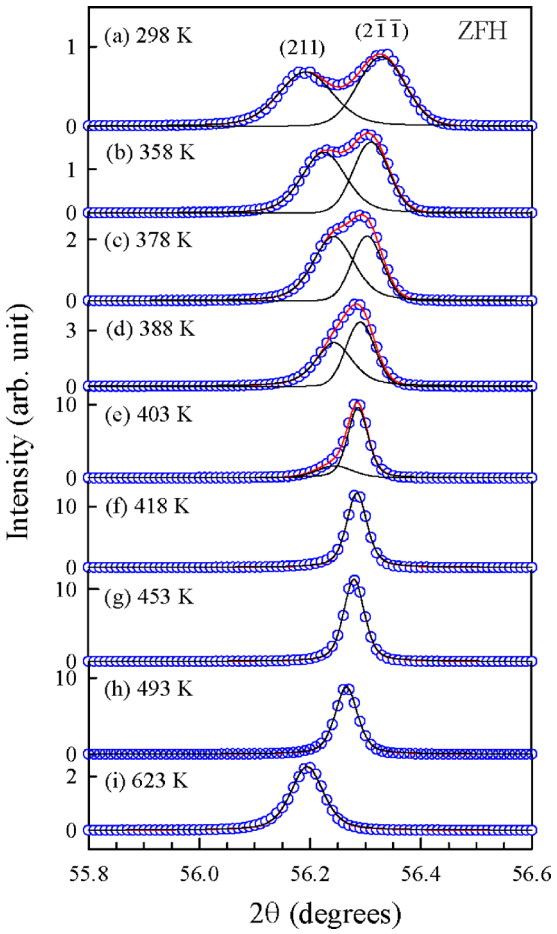


FIG. 4. (Color online) ZFH (211) XRD spectra. The red solid line is the sum of fitting curves.

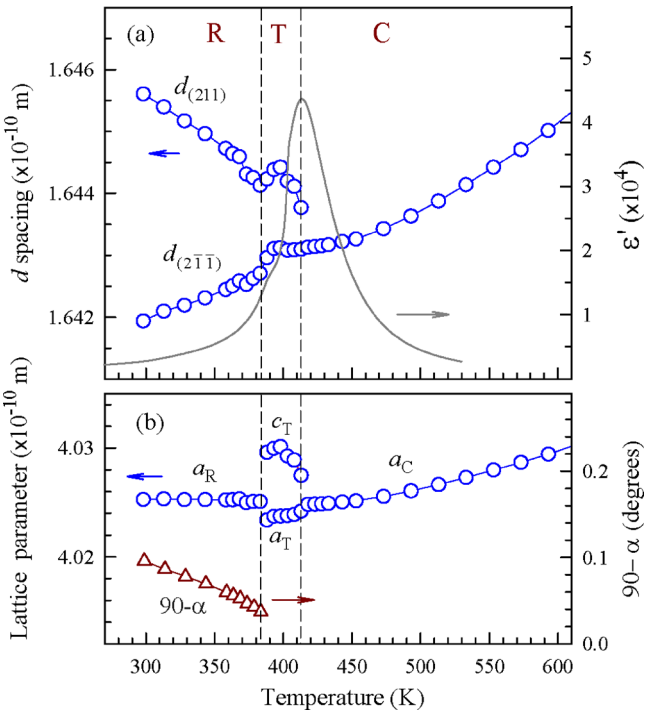


FIG. 5. (Color online) (a) $d$ spacing and (b) lattice parameters obtained from the ZFH (211) XRD. The background is $\varepsilon'_{ZFH}$. The dashed lines indicate transition temperatures.

tion ordering due to change in ion displacement. This can explain the discontinuous responses in $\varepsilon'_{PP\text{-}ZFH}$ and $J_{ZFH}$ near 365 K. The drop from maximum plateau near 365 K in polarization (Fig. 3) also suggests a polarization transition in the R phase. The XRD spectrum changes near 375 K, indicating a R–T transition. The significant decline in $P_r$ near 375 K supports appearance of T polarization, because [001] T polarization has less component along the [211] measuring field, as discussed above. Upon further heating, the slope of $d$ spacing exhibits a change near 415 K as seen in Fig. 7(a), confirming a T–C phase transition. The $d$ spacing of C phase gradually rises due to thermal expansion. In brief, the (211) poled PMN–30%PT crystal undergoes a R–T–C transition sequence near 375 and 415 K upon zero-field heating. In addition, a sharp but relatively minor anomaly near 365 K in $\varepsilon'_{PP\text{-}ZFH}$ and $J_{PP\text{-}ZFH}$ is caused by a transition of R phase polarization ordering.

Figure 8 shows direct (or normal) piezoelectric coefficient $d_{33}$ as a function of poling $E$ field at room temperature. The $d_{33}$ exhibits a rapid increase at $E=1.0-1.3$ kV/cm and reaches a maximum of ~300 pC/N near $E=1.3$ kV/cm, followed by an overpoling behavior characterized by a reduction in piezoelectric coefficient with increasing field. A similar but more significant increase in $d_{33}(\cong 1600$ pC/N) at $E=1-2$ kV/cm was obtained from the (001) PMN–30%PT crystal.[21] To understand what is responsible for the rapid increase in $d_{33}$, the (211) synchrotron XRD spectra before and after poling at $E=5.0$ kV/cm along [211] are plotted in Fig. 9. The (211) peak was enhanced significantly and shifted toward lower $2\theta$ after poling, indicating a larger $d$ spacing or ion displacement. The half-width at half-height also becomes

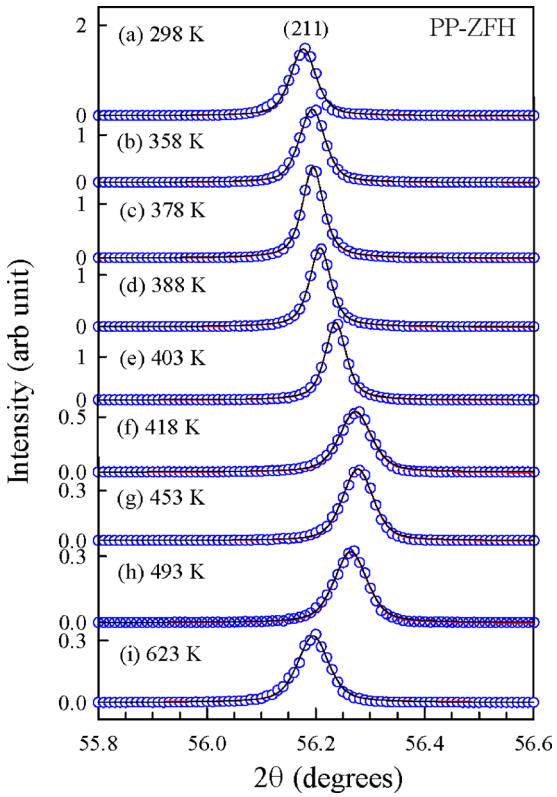


FIG. 6. (Color online) PP-ZFH (211) XRD spectra.

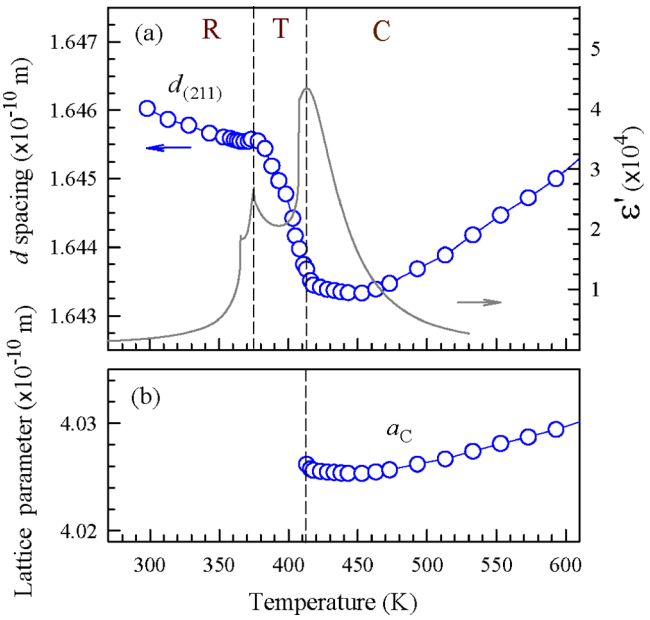


FIG. 7. (Color online) (a) $d$ spacing and (b) lattice parameters obtained from the PP-ZFH (211) XRD. The background is $\varepsilon'_{\text{PP-ZFH}}$.

narrower after poling. It suggests that actual polarization and domain size have a significant increase after poling. These results imply that the measured $d_{33}$ can be probably explained by the product of two factors, i.e., $d_{33}=(P_p/P_{sp})d_{33p}$. Here, $P_p$ is the actual polarization of the sample consisting of phase p, $P_{sp}$ is the saturation polarization of a single domain of phase p, and $d_{33p}$ is the piezoelectric coefficient for a completely polarized sample of phase p. $P_p$, $P_{sp}$, and $d_{33}$ values are relative to the axis perpendicular to the cut plane. The rapid increase in $d_{33}$ at $E=1.0-1.3$ kV/cm is mainly due to the increment in the $P_p/P_{sp}$ factor for this (211) PMN–30%PT crystal. Since structure and polarization of relaxor FEs depend on orientation, Ti content, and poling field, the field-induced phase can play an important factor in the lower Ti doped PMN–PT for the rapid increase in $d_{33}$.

## IV. CONCLUSIONS

The (211)-cut unpoled and poled PMN–30%PT crystal undergoes an R–T–C phase sequence upon zero-field heating. A transition of polarization ordering which is responsible for the discontinuous anomalies near 365 K in $\varepsilon'_{\text{PP-ZFH}}$ and $J_{\text{PP-ZFH}}$, was observed before the R–T transition takes place

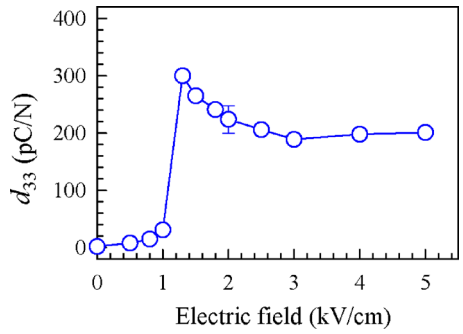


FIG. 8. (Color online) Direct piezoelectric coefficient $d_{33}$ as a function of poling $E$ field.

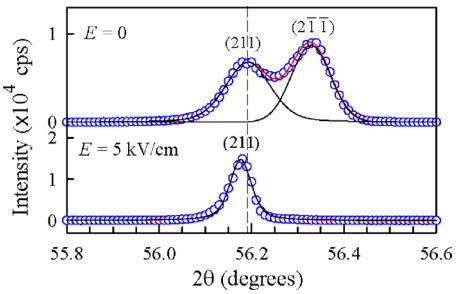


FIG. 9. (Color online) (211) XRD spectra (a) before and (b) after poling at $E=5.0$ kV/cm. The dashed line indicates the shift in diffraction peaks.

in the poled crystal. Poling at $E=5.0$ kV/cm at room temperature apparently enhances the (211) domain and its polarization ordering. Both $\varepsilon'_{\text{ZFH}}$ and $\varepsilon'_{\text{PP-ZFH}}$ follow the Curie–Weiss equation above $T_B=510$ K with $C=1.8\times10^5$ K and $T_o=465$ K.

The R–T–C phase sequence in the PP-ZFH process for the (211) PMN–30%PT crystal is essentially different from the R–O–T–C phase sequence observed from a (110)-cut poled PMN–30%PT crystal upon zero-field heating.[22] A $R(R_{NT})-T(T_{NT})-C$ transition sequence was proposed for the (001) poled PMN–30%PT crystal upon zero-field heating.[23] $R_{NT}$ and $T_{NT}$ are R and T nanotwin structures, respectively. These results suggest that the $E$-induced phase or intermediate phase is sensitive to crystallographic orientation. Note that both the outer layer and inner part of PMN–$x$PT crystals ($x\geq27\%$) have the same structure.[6,7] Therefore, the XRD spectra in this work can present the true structure inside the crystal.

The direct $d_{33}$ exhibits a rapid increase for poling field at $E=1.0-1.3$ kV/cm. This study suggests that a significant increment of polarization plays an important role while the high piezoelectric coefficient builds up. A slight overpoling effect was observed in this (211) PMN–30%PT crystal.

## ACKNOWLEDGMENTS

This work was supported by National Science Council of Taiwan Grant No. 97-2112-M-030-003-MY3.

[1]R. Blinc, V. V. Laguta, B. Zalar, and J. Banys, J. Mater. Sci. **41**, 27 (2006).
[2]C. Stock, G. Xu, P. M. Gehring, H. Luo, X. Zhao, H. Cao, J. F. Li, D. Viehland, and G. Shirane, Phys. Rev. B **76**, 064122 (2007).
[3]G. Xu, Z. Zhong, Y. Bing, Z.-G. Ye, C. Stock, and G. Shirane, Phys. Rev. B **70**, 064107 (2004).
[4]G. Xu, P. M. Gehring, C. Stock, and K. Conlon, Phase Transitions **79**, 135 (2006).
[5]G. Xu, H. Hiraka, G. Shirane, and K. Ohwada, Appl. Phys. Lett. **84**, 3975 (2004).
[6]P. M. Gehring, W. Chen, Z.-G. Ye, and G. Shirane, J. Phys.: Condens. Matter **16**, 7113 (2004).
[7]G. Xu, D. Viehland, J. F. Li, P. M. Gehring, and G. Shirane, Phys. Rev. B **68**, 212410 (2003).
[8]G. Xu, Z. Zhong, Y. Bing, Z.-G. Ye, C. Stock, and G. Shirane, Phys. Rev. B **67**, 104102 (2003).
[9]H. Cao, J. Li, and D. Viehland, Phys. Rev. B **73**, 184110 (2006).
[10]H. Cao, C. Stock, G. Xu, P. M. Gehring, J. Li, and D. Viehland, Phys. Rev. B **78**, 104103 (2008).
[11]Z. Feng, X. Zhao, and H. Luo, J. Appl. Phys. **100**, 024104 (2006).
[12]Y. Lu, D.-Y. Jeong, Z.-Y. Cheng, Q. M. Zhang, H. Luo, Z. Yin, and D. Viehland, Appl. Phys. Lett. **78**, 3109 (2001).
[13]D. Viehland and J. F. Li, J. Appl. Phys. **92**, 7690 (2002).
[14]M. Shanthi, K. H. Hoe, C. Y. H. Lim, and L. C. Lim, Appl. Phys. Lett. **86**,

262908 (2005).
[15]A. A. Bokov and Z.-G. Ye, Appl. Phys. Lett. **92**, 082901 (2008).
[16]B. D. Cullity, *Elements of X-Ray Diffraction*, 2nd ed. (Addison-Wesley, Reading, MA, 1978), p. 501.
[17]D. Vanderbilt and M. H. Cohen, Phys. Rev. B **63**, 094108 (2001).
[18]K. Hirota, Z.-G. Ye, S. Wakimoto, P. M. Gehring, and G. Shirane, Phys. Rev. B **65**, 104105 (2002).
[19]D. Viehland, S. J. Jang, L. E. Cross, and M. Wuttig, Phys. Rev. B **46**, 8003 (1992).
[20]C.-S. Tu, H.-T. Chuang, S.-C. Lee, R. R. Chien, V. H. Schmidt, and H. Luo, J. Appl. Phys. **104**, 024110 (2008).
[21]C.-S. Tu, C.-M. Hsieh, V. H. Schmidt, R. R. Chien, and H. Luo, Appl. Phys. Lett. **93**, 172905 (2008).
[22]C.-S. Tu, V. H. Schmidt, R. R. Chien, S.-H. Tsai, S.-C. Lee, and H. Luo, J. Appl. Phys. **104**, 094105 (2008).
[23]C.-S. Tu, C.-M. Hsieh, R. R. Chien, V. H. Schmidt, F.-T. Wang, and W. S. Chang, J. Appl. Phys. **103**, 074117 (2008).